



Sub-Chronic Aluminum Exposure in Rats' Learning-Memory Capability and Hippocampal Histone H4 Acetylation Modification: Effects and Mechanisms

Jie Gao¹ · Shiming Zhang¹ · Bing Li² · Ziyi Wang³ · Wei Liu¹ · Lifeng Zhang¹

Received: 26 December 2022 / Accepted: 6 February 2023
© The Author(s), under exclusive licence to Springer Science+Business Media, LLC, part of Springer Nature 2023

Abstract

Aluminum has been found to be closely related to the pathogenesis of neurodegenerative diseases and damage learning and memory functions. Many changes in epigenetics may be one of the mechanisms of aluminum neurotoxicity. The purpose of this study is to further investigate the mechanism of action of sub-chronic aluminum exposure on learning memory and histone H4 acetylation modification in Wistar rats, and the correlation between learning memory impairment and histone H4 acetylation in aluminum-exposed rats. Rats in each dose group were given 0.0 g/L, 2.0 g/L, 4.0 g/L, and 8.0 g/L of AlCl₃ distilled water daily for 12 weeks. The learning and memory ability of rats was measured by the Morris water maze test; the neuronal morphology of rat hippocampus was observed by Nissl staining and transmission electron microscope; real-time PCR, and Western blot were used to detect mRNA expression and protein content in hippocampus of rats. The results suggest that aluminum may affect the gene and protein expression of HAT1 and HDAC2, and then affect histone H4 and the acetylation of H4K12 (acH4K12), which may lead to learning and memory dysfunction in rats.

Keywords Aluminum · Hippocampus · Learning and memory · Histone H4 · Acetylation · Rats

Introduction

Aluminum (Al) is the most plentiful metal element in the earth's crust, third only to oxygen and silicon. Al is widely used in industries, agriculture, medicine, and everyday life due to the rapid growth of the socioeconomic development. Through water, air, food, and vaccines, we are exposed to Al throughout our lives. Al enters the human body through gastrointestinal and respiratory tracts, skin contact, etc. and is eliminated from the body through urine and sweat, but

excessive exposure to Al causes damage to the nerve, blood-forming, skeletal, immune, and other systems [1]. Previous research has shown that Al crosses the blood–brain barrier and accumulates in the entorhinal cortex, hippocampus, inferior colliculus, and diaphragm [2]. The hippocampus is the most sensitive brain region to Al exposure, as it plays a key role in the regulation of learning and memory, and is an important part of neural activity such as emotion and behavior [3]. Hippocampal Al accumulation can lead to nerve cell damage, cognitive dysfunction, abnormal behavior, and even nerve cell degeneration [4, 5]. As a neurotoxin, Al has been implicated in the pathogenesis of many neurodegenerative diseases [6], including amyotrophic lateral sclerosis, Parkinson's disease (PD), and Alzheimer's disease (AD) [7]. Chronic exposure to Al has been shown to cause cognitive dysfunction and decreased learning and memory ability, which is significantly related to the dose of exposure [8–10].

Although the mechanism of Al neurotoxicity is complex, several epigenetic changes may be involved [11]. Epigenetic changes in gene expression are likely to be one of the directions to investigate the pathogenesis of disease. Epigenetics refers to the hereditary changes caused by unaltered DNA sequence but altered genetic expression, mainly including

Jie Gao, Shiming Zhang and Bing Li contributed equally to the presented study.

✉ Lifeng Zhang
zgykdxzlf@163.com

¹ Department of Maternal, Child and Adolescent Health, School of Public Health, Shenyang Medical College, Shenyang, Liaoning 110034, People's Republic of China

² Department of Dermatology, Shengjing Hospital of China Medical University, Shenyang, Liaoning 110004, People's Republic of China

³ Shenyang Pharmaceutical University, Shenyang, Liaoning 110016, People's Republic of China

DNA methylation, histone modification, RNA regulation, and chromatin remodeling, among others. Histone acetylation is a vital histone modification and one of the primary research forms of epigenetic mechanism being studied [12].

Histone acetylation is known to be indispensable for many physiological and biochemical processes in cells, such as gene expression, genome maintenance, and biological development. Histone acetylation is coordinated by histone acetyltransferases (HATs) and histone deacetylases (HDACs) and often occurs at the terminal amino acid residues of histone H3 and H4 subunits, and can activate transcription and promote gene expression. All eukaryotes have several acetyltable lysine residues in the nitrogen-terminal tail of histone H4 that can be acetylated, including K5, K8, K12, and K16. By neutralizing their positive charge, acetylation of lysine residues on histone H4 frees chromatin structures and encourages the combination of various factors, including transcription factors and co-activators [13, 14]. HAT is widely expressed in various tissues and organs. By mediating the transfer of acetyl groups to lysine residues at the end of histone subunits, HAT can increase the level of acetylation of histones, thereby activating the transcription of specific genes, in order to promote HAT to bind acetyl groups to the nitrogen-terminal tail of histones, promote chromosome depolymerization, and activate transcription. HDAC can remove these acetyl groups from the nitrogen-terminal tail of histones, sealing the DNA, and inhibiting transcription process. Under normal circumstances, the protein concentration and enzymatic activity of HAT and HDAC maintain a highly coordinated equilibrium state that is indicative of neuronal homeostasis and is responsible for the regulation of gene expression and the maintenance of normal neurophysiological performance, such as long-term enhancement, learning, and memory [15, 16].

In Germany, a meta-analysis found an exposure–response relationship between AI and cognitive impairment after confounding factors had been excluded [17]. The accumulation of AI in the brain is a well-known industrial environmental neurotoxicant that can exacerbate oxidative and inflammatory processes, which lead to tissue destruction, and has been directly linked to the onset and progression of AD [18, 19]. The genomic location of lysine (H4K16) acetylation changes at position 16 of histone H4 and was associated with the genetic variation and expression of quantitative trait loci identified in genome-wide association studies of AD [20]. Histone acetylation is key to forming memories [21]. The results showed that histone acetylation was related to the protective effects on learning, memory, and the nervous system. The primary mechanism of histone acetylation was that HAT promotes histone acetylation and associated gene transcription, promoting learning, memory, and neuroprotection, whereas HDAC enhances histone deacetylation and

inhibits gene transcription, reducing the capacity of the nervous system [22, 23].

A great quantity of studies have suggested that epigenetic alterations may be the mechanisms of AI neurotoxicity, but there are few reports on histone H4 acetylation changes in sub-chronically AI-exposed rats at home and abroad, which is the starting point of this research.

Materials and Methods

Animals

Healthy and clean mature Wistar rats (220 ± 10 g) were supplied by the Animal Laboratory Centre of Shenyang Medical College. The rats were fed with rat breeding chow (Changsheng Biotechnology Co., Ltd., Liaoning). Light 12 h/day, temperature $18 \sim 23$ °C, relative humidity 45 ~ 55%. The rats were habituated to the environment for a week before mating and the ratio of females to males was 2:1. The copulatory plugs were observed to determine the date of successful mating and conception. Pregnant rats were randomly assigned into four groups of 10 rats each, including three AI-exposed groups and one control group. To simulate the exposure of human infants to AI from lactation to adulthood, the exposure period started from the first day after birth (day 0), female rats in the AI-exposed groups received distilled water solution (containing 2.0 g/L, 4.0 g/L, and 8.0 g/L AlCl_3 , separately), while female rats in the control group continued to drink distilled water. Provide water 24 h a day to imitate the drinking mode of human being. Eliminate rats that are too large or too small and use the random number table method to select the rats to keep 8 animals in each litter and the ratio of male to female was 1:1 as much as possible. Females and males were used alternately for the measurement of each index. The offspring rats were first exposed to AI through breastfeeding within 3 weeks of birth and were self-exposed to distilled water containing AlCl_3 after weaning until 12 weeks after birth. After 12 weeks of AI exposure, the rats were weighed, then one portion of the rats were subjected to a water maze experiment, followed by measurement of brain weight, hippocampal weight, AI content, and biochemical indices, and another portion of the rats were histopathologically observed after live perfusion. In each experiment, rats were selected using a random number table and the sex ratio of the rats used was 1:1.

The guidelines for the care and use of laboratory animals issued by the Shenyang Medical College and the National Institutes of Health were strictly followed in all animal breeding and experimental operations.

Chemicals

All chemicals are guaranteed reagents; main reagents include AlCl_3 crystal (Pharmaceutical Chemical Reagent Co., Ltd., Shenyang, China); anti-rabbit rat HAT1 and HDAC2 antibody, Histone H4 Rabbit pAb, Acetyl-Histone H4-K12 Rabbit pAb, β -Actin antibody and SDS (ABclonal Biotechnology Co., Ltd., Wuhan, China); HRP labeled anti-rabbit IgG antibody, Monzol™ total RNA extraction reagent, MonScript™ RTIII All-in-One Mix and MonAmp™ ChemoHS qPCR kit (Mona Biotechnology Co., Ltd., Wuhan, China); Tar purple Nessler staining kit (BestBio Co., Ltd., Shanghai, China); nuclear protein and plasma protein extraction kit and BCA protein concentration determination kit (Keygen Co., Ltd., Jiangsu, China); SDS-PAGE gel preparation kit (Beyotime Biotechnology Co., Ltd., Shanghai, China); PVDF membrane (Millipore Co., Ltd., Germany); 2×PBST buffer, Glycine acid, and TRIS (Solarbio science & technology Co., Ltd., Beijing, China); Predyed protein Marker (Thermo Co., Ltd., USA). The standard Al reference materials were acquired from the National Standard Reference Material Centre (Beijing China).

Morris Water Maze

The offspring were weighed and subjected to behavioral training and testing in a Morris maze (Stoelting Co., Ltd., USA). The water maze lab was kept quiet with soft and even lighting. The water maze pool was made out of a circular tank (diameter: 120 cm; height: 50 cm) and an escape platform (diameter: 10 cm); the water temperature was maintained at 22 ± 2 °C. The escape platform was submerged 1 cm by injecting water and made opaque by adding edible white pigment. Eight animals were randomly selected from each group. During the training phase, each animal was trained 4 times/day for 5 days. After 5 days of training and 24 h of rest, an experiment was conducted. Prior to the experiment, the rats were placed in a pool (without a platform) and allowed to swim freely for 2 min to familiarize them with the maze environment. Place the rats facing the wall of the bucket in a fixed quadrant and allow the rats to move freely. Allow the rats to stay for 10 s, if they find the platform within 60 s; lead the rats to the escape platform and let them stay for 10 s, if they do not find the escape platform within 60 s. After a week, positioning navigation and space exploration were carried out. Rats were deposited into the pool to carry out the positioning navigation experiment, and the time (Latent period) and the distance (Swimming distance) from the time of placing in the pool to finding the platform were observed; in the space exploration experiment, the escape platform was withdrawn, and the rats were deposited into the pool with the same entry point to observe the time of staying in the right quadrant

of the platform (target quadrant dwell time) and the times of crossing the target platform (crossing times). These four indicators were recorded by ANY-maze video tracking software (Stoelting Co., Ltd., USA) and compared to analyze the performance of the rats.

Determination of Al Content

Hippocampal Al content was determined by inductively coupled plasma mass spectrometry (ICP-MS). Six hippocampi were randomly selected from each group, accurately weighed 0.2 g, placed in a tetrafluoroethylene digestion tube, and added 5 mL of superior pure nitric acid and 1 mL of superior pure hydrochloric acid; the tetrafluoroethylene digestion tube was sealed, then placed in porcelain tube to dissolve the tissue in an ultrahigh-pressure microwave digestion apparatus for about 1 h, and made blank control at the same time. When the tissue was completely dissolved, the sample solution was transferred to a 50 mL volumetric flask containing 20% nitric acid, and the sample solution was kept at a constant volume of 50 mL. The final Al ion content of the hippocampus of each rat was equal to the measured Al content minus the background value of the blank control.

Hippocampus Coefficient and Brain Coefficient

Hippocampal coefficient is the percentage of hippocampal weight to body weight; brain coefficient is the percentage of brain weight to body weight.

Ultrastructural Observation of Hippocampal Neurons and Synapses

Eight rats in each group were selected by the random number table method, anesthetized with 1% sodium pentobarbital (40 mg/kg), and the hearts were exposed by thoracotomy and perfused sequentially with 0.9% sodium chloride solution and 2% paraformaldehyde-2.5% glutaraldehyde fixative (pH=7.4) for 30 min through the left ventricle-ascending aorta cannula. The hippocampus was quickly dissected on the ice surface, and 1 mm³ of tissue from CA1 and CA3 was fixed with 2.5% glutaraldehyde phosphate buffer (the temperature of the fixing solution was maintained at 0~4 °C); further, it was rinsed with PBS (pH=7.2~7.4) for 3 times, 10 min/time, 1% samarium tetra-oxide was fixed for 15 h, rinsed 3 times with PBS for 10 min/time, dehydrated in gradient ethanol, embedded, polymerized at 60 °C for 72 h. Then the samples were sectioned at 70 μm slices and stained with Uranil acetate and lead citrate. Finally, hippocampal synapse and neuronal ultrastructure were observed and photographed by transmission electron microscope (H-600-4, Hitachi Co, Japan) (magnification $\times 20$ k and $\times 50$ k).

Nissl Staining

Eight rat brain tissues were taken from each group and preserved in 4% paraformaldehyde. The tissues were trimmed to expose the hippocampus and rinsed under running water overnight. The next morning, alcohol gradient dehydration was started, each gradient was 1 h, and xylene was dealcoholized 3 times, 30 min each time. Paraffin wax was dissolved in three wax cups. After tissue dealcoholization, wax was immersed in each wax cup for 30 min and embedded using a paraffin embedding machine (Leica Co., Ltd., Germany). Using a paraffin sectioning machine, tissues were cut into 4- μ m-thick paraffin sections and taped to the middle and bottom of the slides. Soaking in sequence to dewax: toluene (I) and xylene (II) at 37 °C for 10 min; absolute ethanol (I) and absolute ethanol (II) for 10 min; 95% ethanol, 90% ethanol, 80% ethanol, and 70% ethanol for 5 min; then 1% tar purple dye solution was stained and differentiated in 56 °C thermostats (Yiheng Co., Ltd., Shanghai, China) for 1 h. After rapid washing with distilled water and rapid dehydration with anhydrous ethanol, transparent and sealed, the hippocampal nerve cells of each dose group were observed and photographed under the microscope (Nikon Co., Ltd., Japan) after drying. Finally, the morphology of hippocampal neurons in each dose group should be recorded and preserved.

Real-Time PCR

The hippocampus of 6 rats in each dose group was homogenized with 50 mg. RNA was extracted according to the instructions of the total RNA extraction kit, then RNA quantification and purity identification were performed. Double-distilled water (ddH₂O) was used as the reference solution to measure the optical density ratio of RNA at 260 nm and 280 nm by spectrophotometer (Thermo Co., Ltd., USA), and the total RNA concentration was recorded. Using total RNA as a template, cDNA was synthesized by reverse transcription and the obtained cDNA was quickly placed on ice for subsequent experiments. Then, configured with a 20 μ L PCR reaction system, the reaction conditions were as follows: pre-denaturation at 95 °C for 10 min, denaturation at 95 °C for 10 s, annealing and extension at 60 °C for 30 s, 40 cycles; dissolve curves were obtained by the instrument default acquisition program. The 7500 fast real-time quantitative PCR instrument (ABI Co., USA) was used for analysis, and the $2^{-\Delta\Delta C_t}$ method was used to calculate the relative expression level of HAT1 mRNA and HDAC2 mRNA with GAPDH as an internal reference. Each experiment was set up with 3 holes and repeated for 3 times. Primer sequences for each gene and GAPDH are listed in Table 1 in the supplemental material.

Western Blot

Nuclear and cytoplasmic proteins were extracted from hippocampal tissue of rats in each dose group according to the kit instructions. The entire extraction process was performed on the ice, and a small amount was packaged for protein concentration determination. The rest was packaged and stored at – 80 °C. The protein concentration of each group was determined by BCA protein quantitative method, the samples were incubated at 37 °C for 30 min without light, and the enzyme marker was set at 562 nm to determine the absorbance value of the samples. The standard curve was plotted to calculate the protein concentration of each sample and adjusted it to 3 or 5 μ g/ μ L. 5 \times loading buffer was added at a ratio of 4:1, mixed, placed in a 100 °C constant temperature metal bath (Thermo Cell, Bioer Technology Co., Ltd., Hangzhou, China) for 8 min, and stored at 4 °C for later use. Then, the solidified adhesive was transferred to the electrophoresis tank and a new configuration of running buffer was added inside and outside the electrophoresis tank in a state of high inside and low outside to form a voltage difference. Proteins were isolated by SDS-PAGE electrophoresis and then transferred to PVDF membrane at a voltage of 100 V. The membrane was placed in 5% nonfat dry milk sealing solution and sealed for 2 h. The PVDF membrane was rinsed in PBST for 30 min and primary antibodies were added: rabbit anti-HAT1 (1:1000), rabbit anti-HDAC2 (1:1000), rabbit anti-histone H4 (1:100), rabbit anti-acetylated histone H4K12 (1:100), and rabbit anti- β -actin (1:2000), and shaken for 1 h and overnight at 4 °C. The following day, the membrane was rinsed with PBST for 30 min and then secondary antibody (1:10,000) hybrid solution was added and shaken for 1 h. Protein bands were observed with ECL chemiluminescence detection reagent and radioautography and grayscale values were analyzed with Quantity one 4.6.2 software.

Statistical Analysis

All of the experimental data were analyzed using SPSS 25.0 (SPSS Co., Ltd. Armonk, NY, USA); normality and homogeneity of variance tests were carried out prior to data analysis, and all data were reported as $\bar{x} \pm s$. For the differences between comparison groups, one-way ANOVA with completely random design was used; two-factor repeated measures analysis of variance was used to compare the repeated design data, LSD-t analysis was used for pairwise comparison, and the correlation was examined using Pearson's correlation coefficient (r), with the test level $\alpha = 0.05$ (bilateral).

Results

Effect of Al on the Body Weight of Rats

Al-L was used for the low-dose group, Al-M for the medium-dose group, and Al-H for the high-dose group, and the results are shown below. The body weight of the rats increased with time; it decreased as the dose of Al increased (Fig. 1). The body weight of rats had statistical significance in the main effect of exposure time, the interaction effect of exposure time and exposure dose, and the main effect of exposure dose ($F=490.762, 11.996, 84.424$, respectively; $P<0.05, P<0.05, P<0.05$), according to repeated ANOVA.

Effects of Al on Hippocampus Coefficient and Brain Coefficient

The brain coefficient of the rats increased as the exposure dose was raised (Fig. 2), that in the Al-exposed groups was higher than that in the control group, and that in the Al-H group was significantly higher than that in the Al-L and Al-M groups, with statistical significance ($F=114.469, P<0.01; P<0.01; P<0.01$). The hippocampal coefficient of rats increased with increasing exposure dose, and the difference between Al-M group and control group, Al-H group and control, and Al-L groups was statistically significant ($F=13.086, P<0.01; P<0.05; P<0.05$).

Effects of Al on Learning and Memory in Rats

The trajectory of the rats in the Morris water maze is shown in Fig. 3. The navigation experiment (Fig. 4) revealed a positive correlation between the average escape

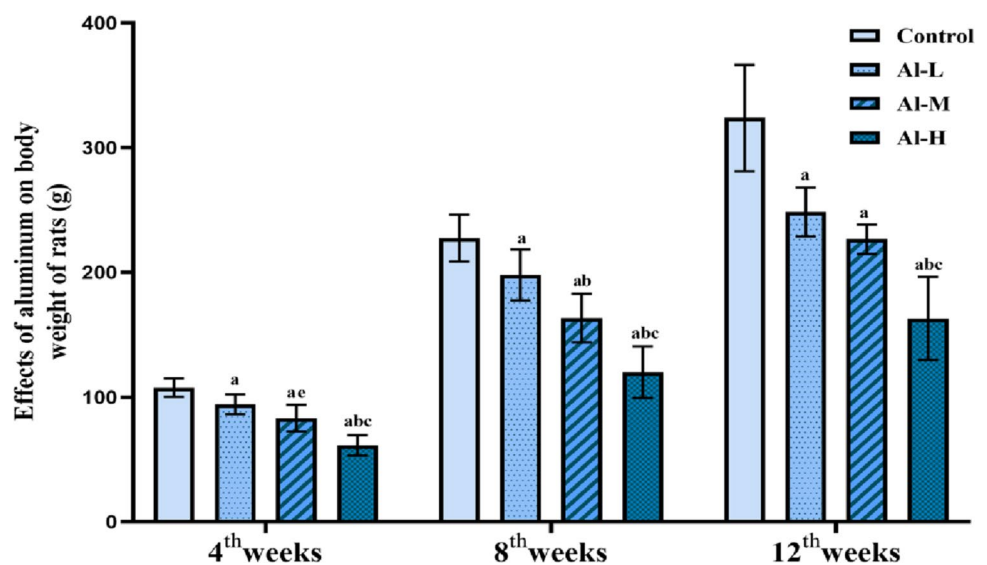
latency and dose ($r=0.971, P<0.01$), with the average escape latency in the Al-exposed groups being higher than that in the control group ($F=588.891, P<0.01$). The mean escape latency in the Al-H group was higher than that in the Al-L and Al-M groups, with statistical significance ($P<0.01; P<0.01$). The swimming distance of rats in the Al-exposed groups was longer than that of the control group ($F=235.181, P<0.01$), the Al-H group was significantly longer than that of the Al-M and Al-L groups, and the Al-M group was longer than that of the Al-L group, with statistical significance ($P<0.01; P<0.01; P<0.01$), and the swimming distance was positively correlated with dose ($r=0.965, P<0.01$).

Spatial exploration showed that the target quadrant dwell time of the Al-exposed groups was shorter than that of the control group ($F=95.464, P<0.01$), and the target quadrant dwell time was negatively correlated with exposure dose ($r=-0.934, P<0.01$). The residence time of the Al-H group was lower than that of the Al-M and Al-L groups, with statistical significance ($P<0.01; P<0.01$). The number of crossing times in the Al-exposed groups was significantly lower than that of the control group ($F=25.232, P<0.01$), and the number of crossing times was negatively correlated with exposure dose ($r=-0.838, P<0.01$). The number of crossing times in the Al-H group was lower than that in the Al-L group, with statistical significance ($P<0.01$).

Results of Al Content in the Hippocampus of Rats

Figure 5 showed that the content of Al in the hippocampus of rats in Al-exposed groups was higher than that in the control group ($F=379.806, P<0.01$), and the content of Al was positively correlated with the exposure dose ($r=0.985$,

Fig. 1 Effects of Al on body weight of rats. ^a $P<0.01$, ^d $P<0.05$ vs. control group, ^b $P<0.01$, ^e $P<0.05$ vs. Al-L, ^c $P<0.01$ vs. Al-M



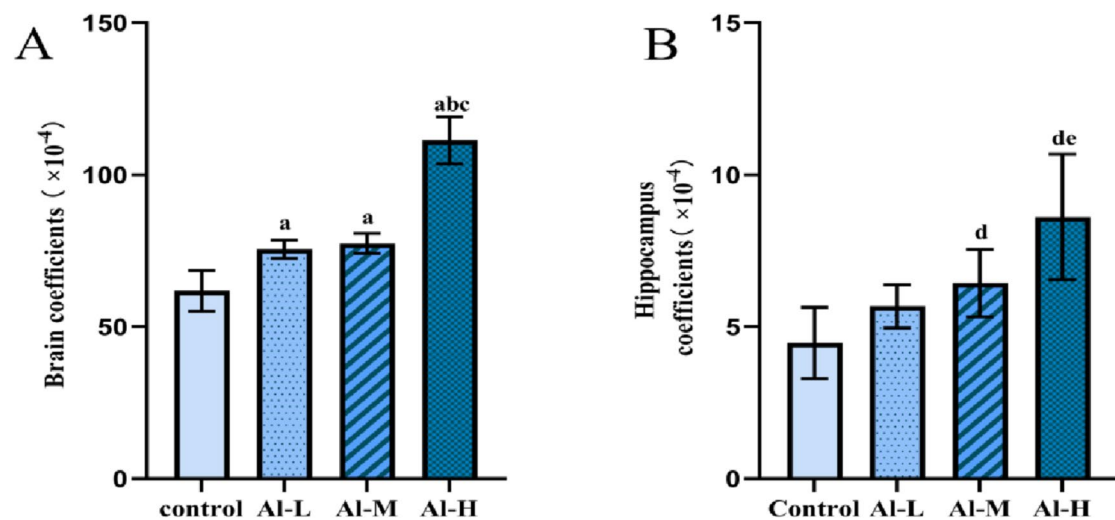


Fig. 2 Effects of Al on brain and hippocampus coefficients in rats. ^a $P < 0.01$, ^d $P < 0.05$ vs. control group, ^b $P < 0.01$, ^e $P < 0.05$ vs. AI-L, ^c $P < 0.01$ vs. AI-M

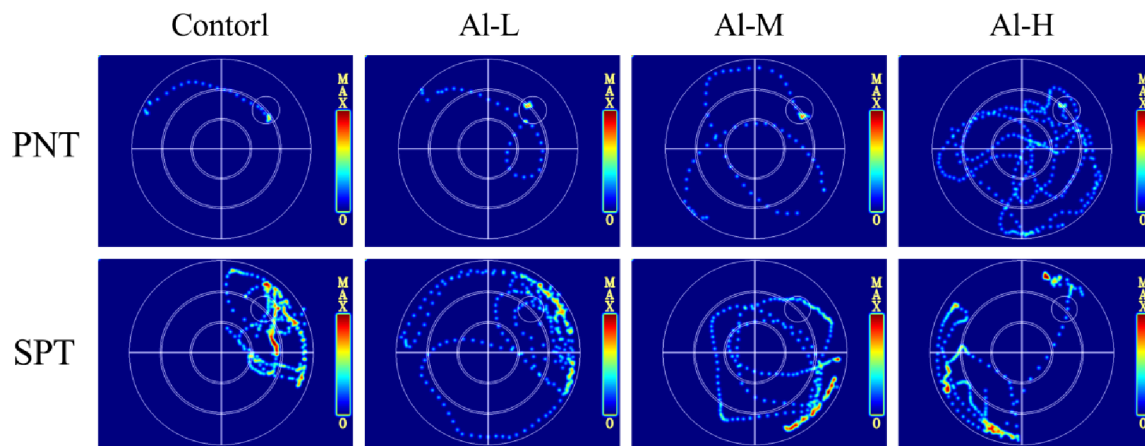


Fig. 3 The search trajectory of rats in the Morris water maze

$P < 0.01$). The content of Al in the AI-M group was higher than that in the control group and the AI-L group ($P < 0.01$; $P < 0.01$), and that in the AI-H group was higher than that in the other three groups, with statistical significance ($P < 0.01$; $P < 0.01$; $P < 0.01$).

Effects of Al on the Morphology of Neurocyte in the CA1 and CA3 Regions of the Hippocampus of Rats

The hippocampus is a significant part of the brain's limbic system, which is responsible for processing key information for learning and memory. Under the interference of external factors, CA1 and CA3 regions are most prone to morphological changes and tissue structure damage. Figure 6 showed that the nerve fibers in the control group

were arranged in order, the neuronal morphology and structure were complete and clear, and the Nissl bodies were abundant and obvious, which was purple-blue. The nerve cells were clear, the number of Nissl bodies was large, and the cytoplasm was rich in Nissl bodies. The glial cells were scattered among the hippocampal neurons, in the shape of stars or fusiform, with small volume and round or oval nuclei, and the nucleus was centered and the nucleolus was obvious. The results suggested that the protein synthesis activity was active in the CA1 and CA3 regions of the hippocampus. As the dose of Al exposure increased, it was observed that the neurocyte was damaged, the nerve fiber space was enlarged, the normal shape of nerve cells was decreased, the arrangement of cells was sparse, the staining was changed from deep to shallow, weakened, nuclear pyknosis, even cell loss, and the volume of the gelatinous fine cell body enlarged

Fig. 4 Effect of Al on learning and memory ability of rats. ^a $P < 0.01$ vs. control group, ^b $P < 0.01$ vs. Al-L, ^c $P < 0.01$ vs. Al-M

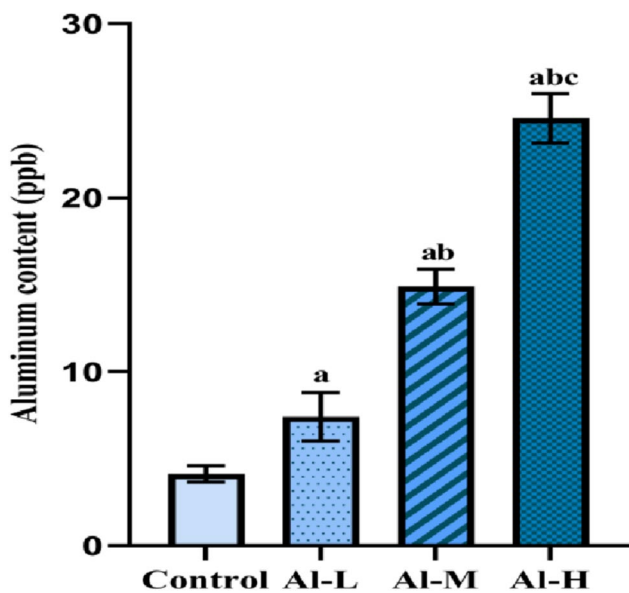
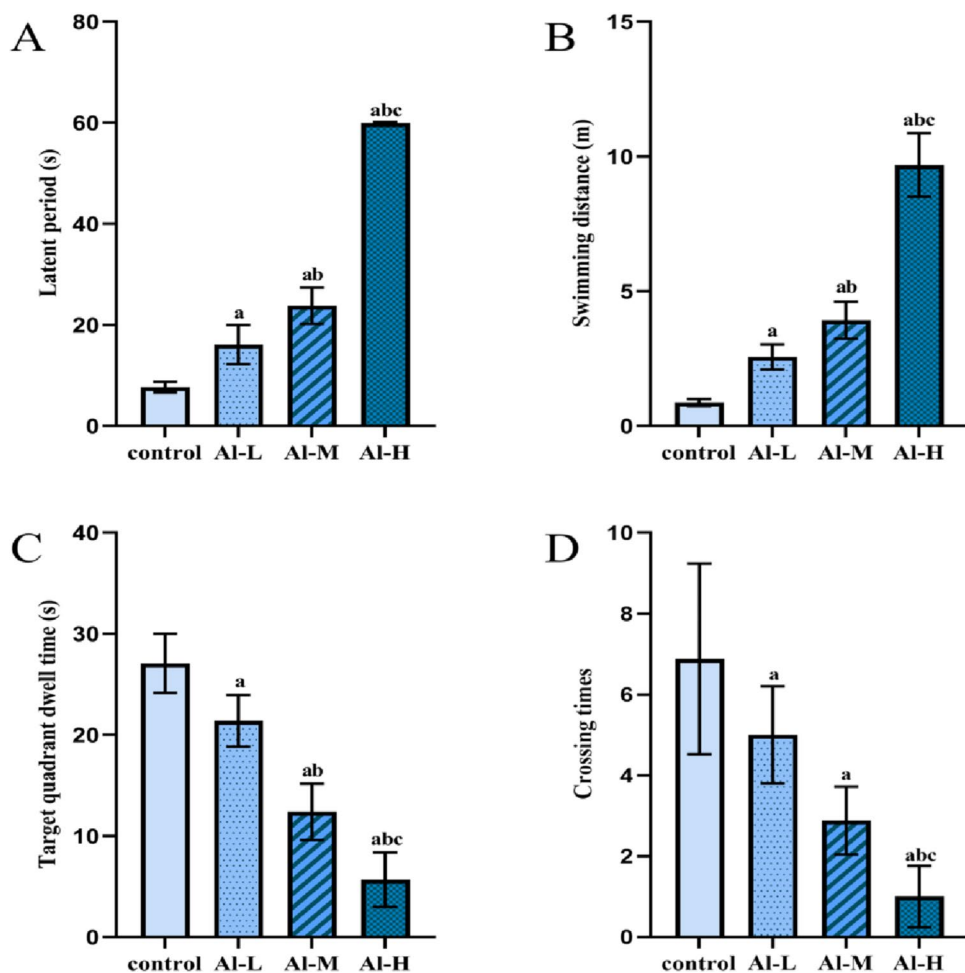


Fig. 5 Al content in hippocampus of rats in each dose group. ^a $P < 0.01$ vs. control group, ^b $P < 0.01$ vs. Al-L, ^c $P < 0.01$ vs. Al-M

and the number increased. The results suggested that sub-chronic Al exposure leads to neurocyte damage in the CA1 and CA3 regions of the rat hippocampus, which leads to decreased learning and memory function in rats.

Effects of Al on Ultrastructure of Hippocampal Neurons and Synapses

The morphology of neurons in the control group was complete, the structure of nuclei and organelles was clear, the euchromatin was abundant, the endoplasmic reticulum and mitochondria were rougher in the cytoplasm, the nucleus was larger, the membrane was obvious, and the nucleolus was more. The morphology of hippocampal neurons was damaged with increasing dose of Al exposure (Fig. 7). In the Al-exposed groups, the nuclei of neurons shrank, the nucleoli disappeared, the mitochondria swelled, the crest was disturbed, the rough endoplasmic reticulum expanded, some organelles vacuolated, and heterochromatin increased. The control group had dense hippocampal synapses and a clear synaptic structure. The hippocampal synaptic

Fig. 6 Nissl staining of CA1 and CA3. **A** Control group; **B** AI-L; **C** AI-M; **D** AI-H (bar = 50 μ m)

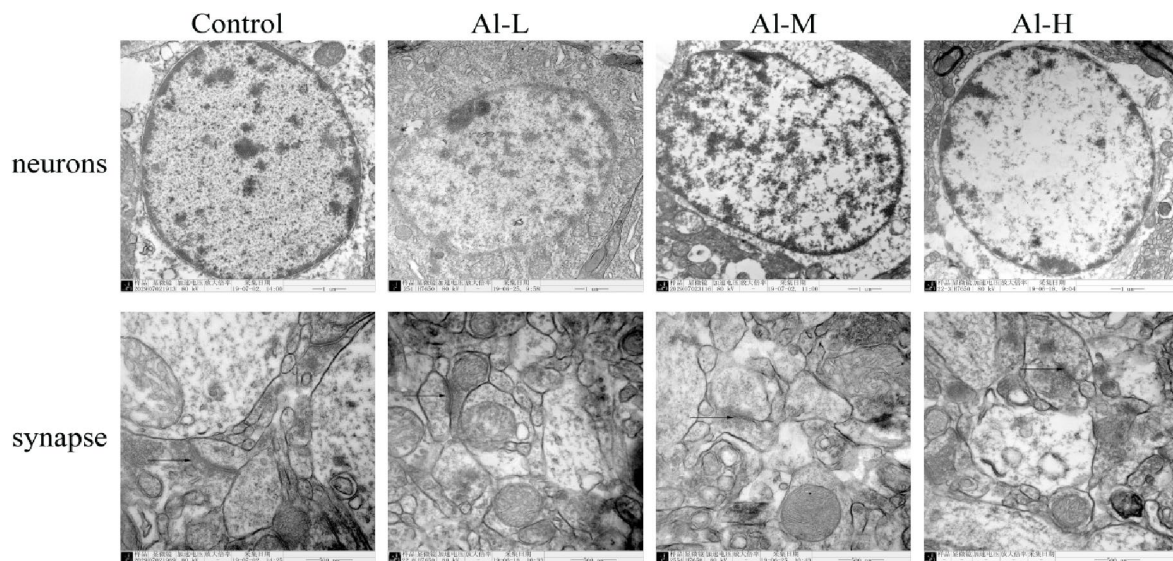
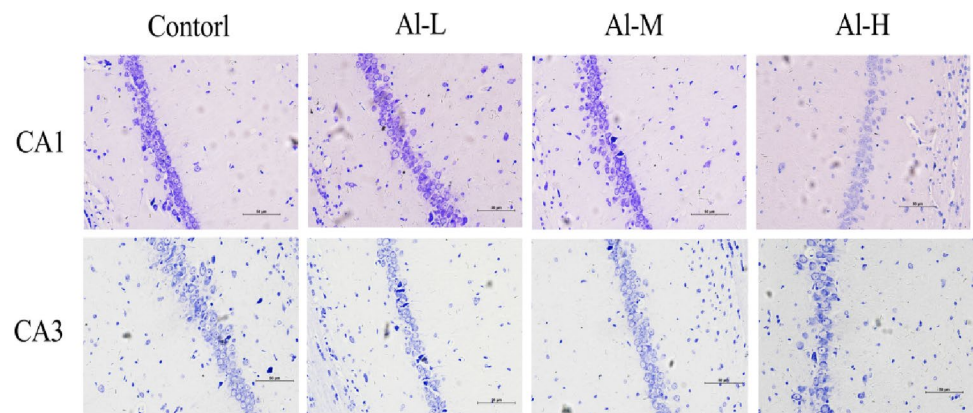


Fig. 7 Ultrastructure of neurons and synapses in hippocampal tissue of each dose group (neurons: $\times 20$ k; synapse: $\times 50$ k)

structure changed with increasing AI dose. The hippocampal synaptic structure became shorter, it was not dense, and the synapses were shallow and short. According to the results, the ultrastructural damage to hippocampal neurons and synapses became more apparent as the AI exposure dose was increased.

Effects of AI on HAT1, HDAC2 mRNA Expression Levels in Hippocampus

Figure 8 demonstrated that HAT1 and HDAC2 mRNA expression levels varied significantly between dose groups ($F = 15.889$, $P < 0.01$; $F = 9.58$, $P < 0.01$). There was a negative correlation between the expression level of HAT1 mRNA and the AI exposure dose ($r = -0.794$, $P < 0.01$). HAT1 mRNA expression in the AI-exposed groups was significantly lower than that in the control group, with statistical significance ($P < 0.05$; $P < 0.01$; $P < 0.01$). There

was a positive correlation between the expression level of HDAC2 mRNA and the AI exposure dose ($r = 0.673$, $P < 0.01$), the expression level of HDAC2 mRNA in the AI-H group was higher than that in the control and AI-L groups, with statistical significance ($P < 0.05$; $P < 0.05$).

Effects of AI on HAT1, HDAC2, H4 and acH4K12 Protein Expression Levels in Hippocampus

Figures 9 and 10 demonstrated statistically significant differences in protein expression of HAT1, HDAC2, H4, and acH4K12 in each dose group ($F = 14.362$, $P < 0.01$; $F = 3.418$, $P < 0.01$; $F = 15.038$, $P < 0.01$; $F = 3.794$, $P < 0.01$). There was a negative correlation between exposure dose and the protein levels of HAT1, H4, and acH4K12 ($r = -0.810$, $P < 0.01$; $r = -0.800$, $P < 0.01$; $r = -0.547$, $P < 0.01$). HAT1 protein content in the AI-exposed groups was lower than that in the control group, with statistical significance ($P < 0.05$; $P < 0.01$);

Fig. 8 HAT1 and HDAC2 mRNA expression levels of rats in each dose group. **A** ^a $P < 0.01$, ^d $P < 0.05$ vs. control group; $n = 6$; **B** ^d $P < 0.05$ vs. control group, ^e $P < 0.05$ vs. Al-L; $n = 6$

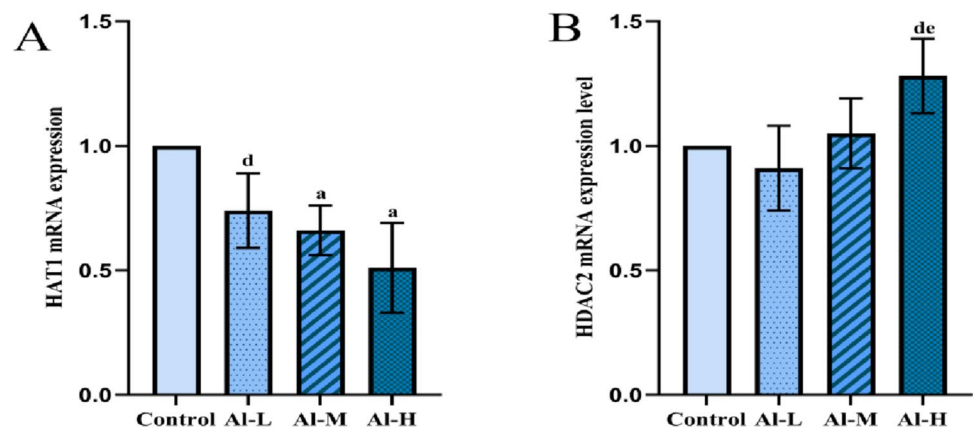
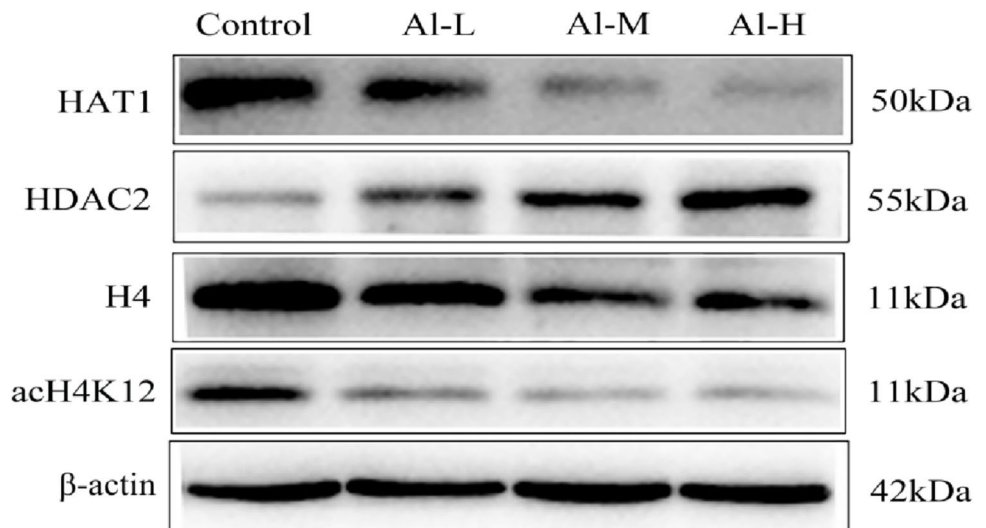


Fig. 9 HAT1, HDAC2, H4, and acH4K12 protein content in hippocampus of rats in each dose group



$P < 0.01$). H4 protein content in the Al-H group was lower than that in the control and Al-L groups, and that in the Al-M group was lower than that in the control group, with statistical significance ($P < 0.01$; $P < 0.05$; $P < 0.05$). The acH4K12 protein content level in the Al-H group was observably lower than that in the control group, with statistical significance ($P < 0.05$). There was a positive correlation between the exposure dose and the protein content of HDAC2 ($r = 0.570$, $P < 0.01$). The HDAC2 protein content in the Al-H group was observably higher than that in the control group, with statistical significance ($P < 0.05$).

Discussion

The experimental results showed that the weight gain of rats in the Al-exposed groups was apparently lower than that of the control group by AlCl_3 solution simulated by human drinking water, and the mean weight of rats in the control group was greater than that of the Al-exposed groups. The

brain and hippocampal coefficients increased with increasing dose of Al. In the Morris water maze experiment, the results of position navigation showed that the escape latency and swimming distance of rats in the Al-exposed groups were higher than those in the control group, and the dwell time and effective crossing times of rats in the Al-exposed groups in the spatial exploration experiment were also shorter than those of the control group, which demonstrated that Al exposure affected the animals' learning and memory abilities. The results of Nissl staining showed that the control group was rich in Nissl substance, with more Nissl substance and deeper staining. The decrease of Nissl substance in the Al-exposed groups indicated the decrease of protein synthesis activity in the hippocampus. Weakened synaptic structures and changes in neuronal morphology in the hippocampus were observed by transmission electron microscopy. These results suggested that Al exposure caused damage to the central nervous system in rats, which presumably resulted in impaired gene expression and protein synthesis within the central nervous system, which in turn caused neurobehavioral abnormalities in the rats.

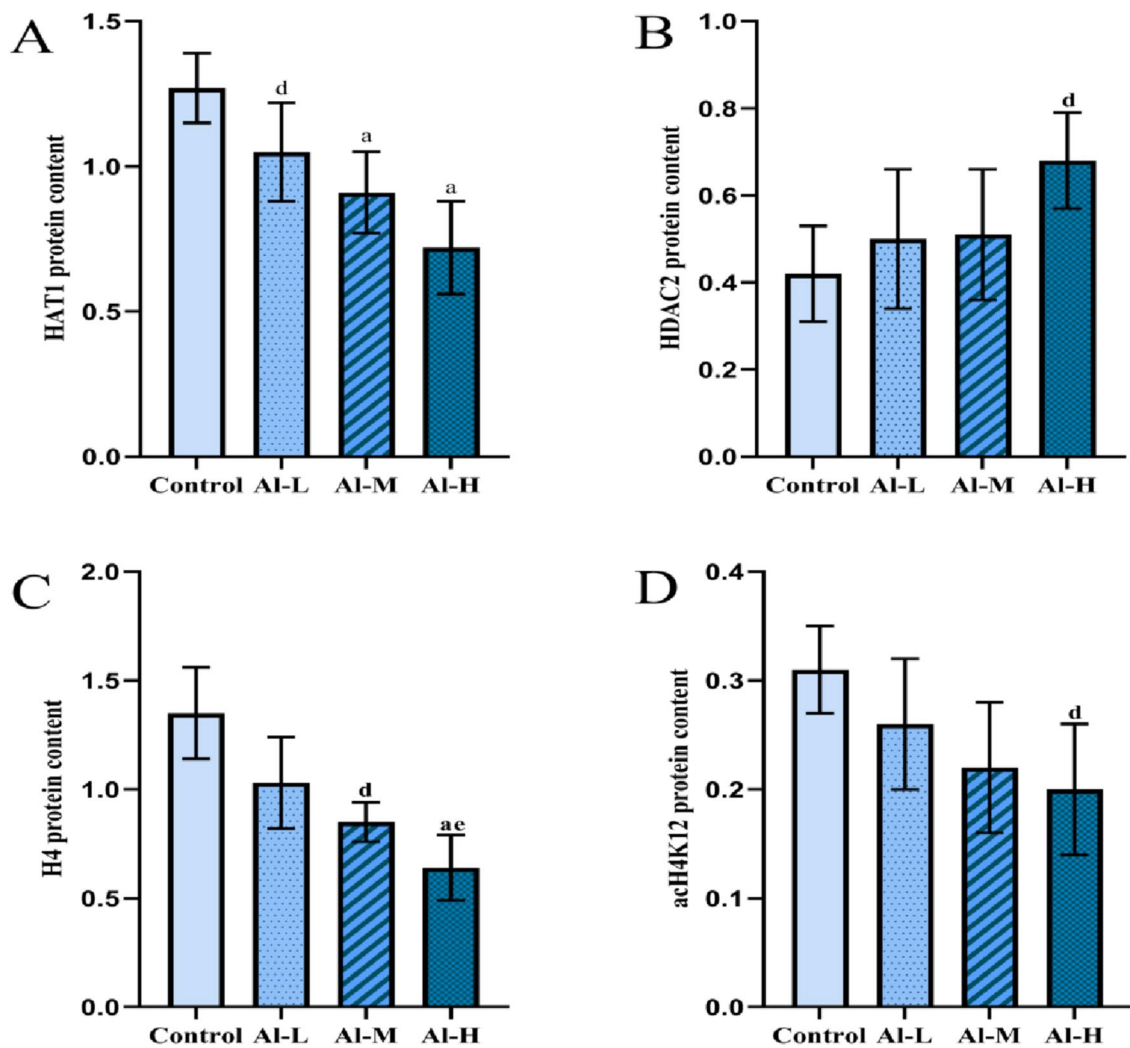


Fig. 10 HAT1, HDAC2, H4, and acH4K12 protein content in hippocampus of rats in each dose group. **A** ^a $P < 0.01$, ^d $P < 0.05$ vs. control group; $n = 6$; **B** ^d $P < 0.05$ vs. control group, $n = 6$; **C** ^d $P < 0.05$ vs. control group, ^c $P < 0.05$ vs. AI-L; $n = 6$; **D** ^d $P < 0.05$ vs. control group; $n = 6$

Histone modifications include methylation, acetylation, phosphorylation, ubiquitination, and ADP-nucleotidylation of histones [24]. Gene regulation was crucially influenced by the enzymes that control this process, and the disruption of signaling pathways resulted in a number of human neurological disorders, including PD, AD, and Huntington's disease [25], which were fundamentally involved in a variety of cellular processes, from regulation of gene expression to DNA damage repair. Histone acetylation is controlled by HATs and HDACs [26], and mediated by HATs. In contrast, HDACs remove acetyl groups from the amino terminus of acetylated histones to resist the effects of HATs and restore histones to their basal state [27]. H4 acetylation is also critical for chromatin structure, gene expression, cell polarization, and cytokine production [28, 29]. HAT1 is responsible for acetylating histones during chromatin assembly, and it is a major acetyltransferase. HAT1 promotes

gene transcription, learning, and memory [30]. HAT1 is acetylated at histone H4K12 and has been implicated in the aging process. In the rat hippocampus, increased acetylation of H4K12 is associated with learning and memory. Treatment with HDAC inhibitors could increase the acetylation of H4 lysine 12 and restore the learning and memory in older mice [31]. In addition, Ito's team found that HDAC2 reduced acetylation of histone H4 at lysine 8 and 12. Increased HDAC2 and inhibited expression of learning and memory genes, such as synapsin 1, resulted in impaired ability to learn and memory [32]. Researches showed that HDAC inhibitors can restore histone acetylation in the hippocampus and thereby improve cognition [33, 34]. In HDAC class I (HDAC1/2/3/8) [35], it is possible that nuclear localization of HDAC1 and HDAC2 regulates most of the observed changes in histone acetylation, mainly involving H4 lysine (K residues 5, 8, 12, and 16 [36, 37]. K12

acetylation appears to be one of the more sensitive indicators for HDAC inhibition [38–41]. The findings demonstrated that HDAC2 mRNA and protein expression increased with increasing exposure dose, while HAT1 mRNA and protein expression decreased with increasing exposure dose in the hippocampus of rats exposed to Al. In addition, the content of histone H4 and acH4K12 decreased with increasing exposure dose, which may be because AlCl₃ induced the changes of HAT1 and HDAC2 in hippocampal rats, and then affected the expression of histone H4 and acH4K12. As a result, we hypothesized that Al exposure reduced HAT1 expression and increased HDAC2 expression in the hippocampus of rats, which led to a decrease in the content of histone H4 and acH4K12 protein, ultimately damaging the memory function of rats. The dynamic balance of HATs-HDACs not only maintains the normal transcription of genes, but also affects the function of learning and memory. This connection between HDAC2 and H4K12 is complicated because there are multiple HATs. Therefore, HAT1 is important for establishing a better correlation between HDAC2 and H4 acetylation. We need to explore it deeply and comprehensively.

Conclusion

Sub-chronic exposure to Al increased the content of Al in the hippocampus, damaged the morphology of neurons in the CA1 and CA3 regions of the hippocampus, injured the synaptic ultra-structure in the CA1 and CA3 regions of the hippocampus, and Al may influence the gene and protein expression of HAT1 and HDAC2, and then affect histone H4 and acH4K12, ultimately resulting in the impairment of learning and memory capability in rats.

Supplementary Information The online version contains supplementary material available at <https://doi.org/10.1007/s12011-023-03602-6>.

Acknowledgements The authors sincerely appreciate the support of everyone. Thank the correspondent for guiding the manuscript.

Author Contribution Jie Gao: conceptualization, methodology, software, data curation, writing—original draft, writing—review and editing. Shiming Zhang: methodology, data curation, writing—original draft. Bing Li: methodology, data curation, writing—original draft. Ziyi Wang: methodology, data curation, writing—original draft. Wei Liu: methodology, data curation, writing—original draft. Lifeng Zhang: conceptualization, methodology, writing—review and editing, supervision.

Funding This research was supported by the National Natural Science Foundation of China (81673226); by the Initiated Research Foundation for the Doctoral Program of Science and Technology Department of Liaoning Province, China (201601226); by the Natural Science Foundation of Education Department of Liaoning Province, China (L2015544, LJKZ1146); by the Natural Science Foundation for Innovation and

Entrepreneurship Training Program of Education Department of Liaoning Province, China (201710164000038); by the Natural Science Foundation of Science and Technology Department of Shenyang City, China (17–231-1–44); by the Natural Science Foundation of Shenyang Medical College, China (20153043); by the Natural Science Foundation for graduate students of Shenyang Medical College, China (Y20180512); and by the Natural Science Foundation for undergraduate students of Shenyang Medical College, China (20179028).

Data Availability The datasets used and/or analyzed during the current study are available from the corresponding author on reasonable request.

Declarations

Disclosure Statement The authors acknowledge that they have read the Journal's position on ethical publishing issues and certify that this manuscript conforms to the Journal's guidelines.

Competing Interests The authors declare no competing interests.

References

1. Yousef MI, Roychoudhury S, Jafaar KS, Slama P, Kesari KK, Kamel MA (2022) Aluminum oxide and zinc oxide induced neurotoxicity in rat brain, heart, and lung. *Physiol Res*. 71(5):677–694. <https://doi.org/10.33549/physiolres.934831>
2. Walton JR (2009) Functional impairment in aged rats chronically exposed to human range dietary aluminum equivalents. *Neurotoxicology* 30(2):182–193. <https://doi.org/10.1016/j.neuro.2008.11.012>
3. Platt B, Fiddler G, Riedel G et al (2001) Aluminium toxicity in the rat brain: histochemical and immunocytochemical evidence. *Brain Res Bull* 55(2):257–267. [https://doi.org/10.1016/S0361-9230\(01\)00511-1](https://doi.org/10.1016/S0361-9230(01)00511-1)
4. Niu Q (2018) Overview of the relationship between aluminum exposure and health of human being. *Adv Exp Med Biol*. 1091:1–31. https://doi.org/10.1007/978-981-13-1370-7_1
5. Sun W, Li J, Li X et al (2022) Aluminium oxide nanoparticles compromise spatial memory performance and proBDNF-mediated neuronal function in the hippocampus of rats. 19(1):34. Published 2022 May 10. <https://doi.org/10.1186/s12989-022-00477-8>
6. Abbas F, Eladl MA, El-Sherbiny M et al (2022) Celastrol and thymoquinone alleviate aluminum chloride- induced neurotoxicity: Behavioral psychomotor performance, neurotransmitter level, oxidative -inflammatory markers, and BDNF expression in rat brain. *Biomed Pharmacother*. 151:113072. <https://doi.org/10.1016/j.biopha.2022.113072>
7. Nie J (2018) Exposure to aluminum in daily life and alzheimer's disease. *Adv Exp Med Biol*. 1091:99–111. https://doi.org/10.1007/978-981-13-1370-7_6
8. Zhang L, Jin C, Liu Q et al (2013) Effects of subchronic aluminum exposure on spatial memory, ultrastructure and L-LTP of hippocampus in rats. *J Toxicol Sci* 38(2):255–268. <https://doi.org/10.2131/jts.38.255>
9. Zhang L, Jin C, Lu X et al (2014) Aluminium chloride impairs long-term memory and downregulates cAMP-PKA-CREB signaling in rats. *Toxicology* 323:95–108. <https://doi.org/10.1016/j.tox.2014.06.011>
10. Li H, Xue X, Li Z et al (2020) Aluminium-induced synaptic plasticity injury via the PHF8- H3K9me2-BDNF signalling pathway. *Chemosphere*. 244:125445. <https://doi.org/10.1016/j.chemosphere.2019.125445>

11. Wang F, Kang P, Li Z et al (2019) Role of MLL in the modification of H3K4me3 in aluminium- induced cognitive dysfunction. *Chemosphere* 232:121–129. <https://doi.org/10.1016/j.chemosphere.2019.05.099>
12. Wu Y, Wang R, Liu R, Ba Y, Huang H (2023) The roles of histone modifications in metal-induced neurological disorders. *Biol Trace Elem Res* 201(1):31–40. <https://doi.org/10.1007/s12011-022-03134-5>
13. van Holde K, Zlatanova J (2007) Chromatin fiber structure: Where is the problem now? *Semin Cell Dev Biol*. 18(5):651–658. <https://doi.org/10.1016/j.semcdb.2007.08.005>
14. Conrad T, Akhtar A (2012) Dosage compensation in *Drosophila melanogaster*: epigenetic fine-tuning of chromosome-wide transcription. *Nat Rev Genet* 13(2):123–134. <https://doi.org/10.1038/nrg3124>
15. Saha RN, Pahan K (2006) HATs and HDACs in neurodegeneration: a tale of disconcerted acetylation homeostasis. *Cell Death Differ* 13(4):539–550. <https://doi.org/10.1038/sj.cdd.4401769>
16. Xu H, Ye M, Xia A et al (2022) The Fng3 ING protein regulates H3 acetylation and H4 deacetylation by interacting with two distinct histone-modifying complexes. *New Phytol*. 235(6):2350–2364. <https://doi.org/10.1111/nph.18294>
17. Meyer-Baron M, Schäper M, Knapp G et al (2007) Occupational aluminum exposure: evidence in support of its neurobehavioral impact. *Neurotoxicology* 28(6):1068–1078. <https://doi.org/10.1016/j.neuro.2007.07.001>
18. Campbell A (2002) The potential role of aluminium in Alzheimer's disease. *Nephrol Dial Transplant* 17(Suppl 2):17–20. https://doi.org/10.1093/ndt/17.suppl_2.17
19. Gupta VB, Anitha S et al (2005) Aluminium in Alzheimer's disease: are we still at a crossroad? *Cell Mol Life Sci* 62(2):143–158. <https://doi.org/10.1007/s00018-004-4317-3>
20. Nativio R, Donahue G et al (2018) Dysregulation of the epigenetic landscape of normal aging in Alzheimer's disease. *Nat Neurosci* 21(4):497–505. <https://doi.org/10.1038/s41593-018-0101-9>
21. Shang A, Bieszczad KM (2022) Epigenetic mechanisms regulate cue memory underlying discriminative behavior. *Neurosci Biobehav Rev*. 141:104811. <https://doi.org/10.1016/j.neubiorev.2022.104811>
22. Henry KW, Wyce A et al (2003) Transcriptional activation via sequential histone H2B ubiquitylation and deubiquitylation, mediated by SAGA-associated Ubp8. *Genes Dev* 17(21):2648–2663. <https://doi.org/10.1101/gad.1144003>
23. Kitahara M, Inoue T, Mani H et al (2021) Exercise and pharmacological inhibition of histone deacetylase improves cognitive function accompanied by an increase of gene expressions crucial for neuronal plasticity in the hippocampus. *Neurosci Lett* 749:135749. <https://doi.org/10.1016/j.neulet.2021.135749>
24. Wang S, Zhang X, Wang Q, Wang R (2022) Histone modification in podocyte injury of diabetic nephropathy. *J Mol Med (Berl)*. 100(10):1373–1386. <https://doi.org/10.1007/s00109-022-02247-7>
25. Ramazi S, Allahverdi A, Zahiri J (2020) Evaluation of post-translational modifications in histone proteins: A review on histone modification defects in developmental and neurological disorders. *J Biosci*. 45:135
26. Gao S, Li L, Han X et al (2021) Genome-wide identification of the histone acetyltransferase gene family in *Triticum aestivum*. *BMC Genomics* 22(1):49. Published 2021 Jan 11. <https://doi.org/10.1186/s12864-020-07348-6>
27. Barnes CE, English DM, Cowley SM (2019) Acetylation & Co: an expanding repertoire of histone acylations regulates chromatin and transcription. *Essays Biochem* 63(1):97–107. <https://doi.org/10.1042/ebc20180061>
28. Agalioti T, Chen G, Thanos D (2002) Deciphering the transcriptional histone acetylation code for a human gene. *Cell* 111(3):381–392. [https://doi.org/10.1016/s0092-8674\(02\)01077-2](https://doi.org/10.1016/s0092-8674(02)01077-2)
29. Schübeler D, MacAlpine DM, Scalzo D et al (2004) The histone modification pattern of active genes revealed through genome-wide chromatin analysis of a higher eukaryote. *Genes Dev* 18(11):1263–1271. <https://doi.org/10.1101/gad.1198204>
30. Poziello A, Nebbioso A, Stunnenberg HG, Martens JHA, Carafa V, Altucci L (2021) Recent insights into Histone Acetyltransferase-1: biological function and involvement in pathogenesis. *Epigenetics*. 16(8):838–850. <https://doi.org/10.1080/15592294.2020.1827723>
31. Peleg S, Sananbenesi F, Zovoilis A et al (2010) Altered histone acetylation is associated with age- dependent memory impairment in mice. *Science* 328(5979):753–756. <https://doi.org/10.1126/science.1186088>
32. Ito K, Yamamura S, Essilfie-Quaye S et al (2006) Histone deacetylase 2-mediated deacetylation of the glucocorticoid receptor enables NF-kappaB suppression. *J Exp Med* 203(1):7–13. <https://doi.org/10.1084/jem.20050466>
33. Wu J, Dong L, Zhang M et al (2013) Class I histone deacetylase inhibitor valproic acid reverses cognitive deficits in a mouse model of septic encephalopathy. *Neurochem Res* 38(11):2440–2449. <https://doi.org/10.1007/s11064-013-1159-0>
34. Nieto-Estevéz V, Changarathil G, Adeyeye AO et al (2022) HDAC1 regulates neuronal differentiation. *Front Mol Neurosci* 14:815808. Published 2022 Jan 12. <https://doi.org/10.3389/fnmol.2021.815808>
35. Vandebroek A, Yasui M (2020) Regulation of AQP4 in the Central Nervous System. *Int J Mol Sci*. 21(5):1603. <https://doi.org/10.3390/ijms21051603>
36. Drummond DC, Noble CO et al (2005) Clinical development of histone deacetylase inhibitors as anticancer agents. *Annu Rev Pharmacol Toxicol* 45:495–528. <https://doi.org/10.1146/annurev.pharmtox.45.120403.095825>
37. Fraga MF, Ballestar E et al (2005) Loss of acetylation at Lys16 and trimethylation at Lys20 of histone H4 is a common hallmark of human cancer. *Nat Genet* 37(4):391–400. <https://doi.org/10.1038/ng1531>
38. Ren C, Zhang L, Freitas MA et al (2005) Peptide mass mapping of acetylated isoforms of histone H4 from mouse lymphosarcoma cells treated with histone deacetylase (HDACs) inhibitors. *J Am Soc Mass Spectrom* 16(10):1641–1653. <https://doi.org/10.1016/j.jasms.2005.06.001>
39. Su X, Zhang L, Lucas DM et al (2007) Histone H4 acetylation dynamics determined by stable isotope labeling with amino acids in cell culture and mass spectrometry. *Anal Biochem* 363(1):22–34. <https://doi.org/10.1016/j.ab.2006.12.031>
40. Zhang L, Su X, Liu S et al (2007) Histone H4 N-terminal acetylation in Kasumi-1 cells treated with decapeptide determined by acetic acid-urea polyacrylamide gel electrophoresis, amino acid coded mass tagging, and mass spectrometry. *J Proteome Res* 6(1):81–88. <https://doi.org/10.1021/pr060139u>
41. Li Y, Seto E (2016) HDACs and HDAC inhibitors in cancer development and therapy. *Cold Spring Harb Perspect Med*. 6(10):a026831. <https://doi.org/10.1101/cshperspect.a026831>

Publisher's Note Springer Nature remains neutral with regard to jurisdictional claims in published maps and institutional affiliations.

Springer Nature or its licensor (e.g. a society or other partner) holds exclusive rights to this article under a publishing agreement with the author(s) or other rightsholder(s); author self-archiving of the accepted manuscript version of this article is solely governed by the terms of such publishing agreement and applicable law.